Sixth International Symposium on

Computational Fluid Dynamics

A Collection of Technical Papers

Volume III

September 4-8, 1995
Lake Tahoe, Nevada

A fast 3D unstructured mesh adaption algorithm with time dependent upwind Euler shock diffraction calculations

W.Speares M. Berzins

School of Computer Studies and the Centre for CFD,
University of Leeds, Leeds LS2 9JT, England

Abstract

This paper is concerned with a numerical investigation into time dependent inviscid 3D shock wave diffraction from a region with right angled cuboid cross section through a 2π solid angle. A novel, fast, 3D unstructured tetrahedral mesh adaption algorithm is used, coupled to a Riemann problem based MUSCL type upwind scheme, which generalises to higher order accuracy the first order method of Godunov. Two shock Mach numbers are studied with strong ring vorticies observed for subsonic post shock flow, and the formation of recompression shocks in the supersonic case.

1 INTRODUCTION

In recent years the numerical investigation of the phenomena of shock wave diffraction has generated great interest within the fluid dynamics community, with a number of high quality two dimensional numerical simulations having been performed e.g. [6]. It is natural to want to extend this numerical work into three dimensions to provide additional insight into the complex flow structures which shock diffraction produces. and to make comparisons with available experimental and theoretical results. The significant computational challenge posed by the scale of the 3D problem makes the use of grid adaptation highly desirable for the calculation of high resolution solutions in highly active flow regions.

This paper describes a preliminary numerical study of inviscid shock wave diffraction around a 3D cuboid corner for a range of shock Mach numbers, using the 3D time dependent Euler equations for an ideal gas. A fast and novel 3D unstructured tetrahedral grid adaptation algorithm, based in part on ideas contained in [3],[4],[7] and of the generic node addition or *h-refinement* type, is used to adapt the computational mesh. This is coupled to a higher order extension of the upwind Godunov scheme of the MUSCL type [12] on tetrahedra. Details of the grid adaptation and solver algorithms are given. The numerical regime investigated concentrates on flows with Mach numbers of 1.7 and 3.0, with the shock diffracting outwards from within a region with cuboid cross section through a 2π solid angle. For the case of subsonic post shock flow the diffraction causes the formation of a clear ring vortex structure around the outer edge of the entrance cavity. The behaviour of these compressible inviscid ring vortices is of significant theoretical interest [9], and preliminary measurements are made of the

vortical Mach number and velocity. For the case of supersonic post shock flow the formation of a recompression shock is observed as in the 2D calculation [6].

The paper is organised as follows. In section 2 and 3 we give the equations and describe the numerical solver algorithm respectively. In section 4 we give details of the mesh adaptation algorithm. Section 5 describes the problem and numerical computations. We finish with some concluding remarks.

2 THE EQUATIONS

The numerical algorithms described here apply to the general class of hyperbolic conservation laws of the form:

$$U_t + [F(U)]_x + [G(U)]_y + [H(U)]_z = 0 \tag{1}$$

for three space dimensions (x, y, z) and with time t. The variable $U(x, y, z, t)$ is the vector of conserved variables and the vector functions $F(U)$, $G(U)$ and $H(U)$ the analytic fluxes. For the case of the 3D Euler equations the conserved variables and fluxes may be written as:

$$\begin{bmatrix} \rho \\ \rho u \\ \rho v \\ \rho w \\ E \end{bmatrix}_t + \begin{bmatrix} \rho u \\ \rho u^2 + p \\ \rho uv \\ \rho uw \\ u(E+p) \end{bmatrix}_x + \begin{bmatrix} \rho v \\ \rho uv \\ \rho v^2 + p \\ \rho vw \\ v(E+p) \end{bmatrix}_y + \begin{bmatrix} \rho w \\ \rho uw \\ \rho vw \\ \rho w^2 + p \\ w(E+p) \end{bmatrix}_z = 0 \tag{2}$$

Here ρ represents density, u,v and w the cartesian x, y and z velocity components and E is the total energy. This is defined:

$$E = \frac{1}{2}\rho(u^2 + v^2 + w^2) + e\rho \quad , \quad e{=}e(\rho, p){=}\frac{p}{(\gamma - 1)\rho} \tag{3}$$

where e is the specific internal energy assuming an ideal gas equation of state which closes the system. On account of the need to admit discontinuous solutions such as shock waves and contact surfaces, it should be understood that we investigate weak solutions of the integral form of these equations.

3 NUMERICAL METHOD

The numerical method we employ is a second order accurate, conservative cell-centred finite volume extension of Godunov's Riemann Problem (RP) scheme, based around MUSCL type piecewise linear reconstructions of the primitive variables within each mesh element [12]. If the solution in some element i at time t^n is U_i^n, and is understood to be an numerical approximation to the exact element averaged solution, then the numerical solution at the next time level t^{n+1} is:

$$U_i^{n+1} = U_i^n - \frac{\Delta t}{V_k} \sum_{k=0}^{3} A_k \mathbf{F}_k . \mathbf{n}_k \tag{4}$$

where the sum is over the k faces of the element i. The fluxes $\mathbf{F}_k$ represent the numerical flux function for each element face, termed the element face fluxes, and are determined by the scheme. The $\mathbf{n}_k$ are the outward face unit normal vectors and A_k the face areas. In the case of the well known Godunov scheme these element face numerical

fluxes are constructed from the solution of the local element Riemann Problem (RP) at each element face. The inter-element RP has initial data

$$U(x,0) = \begin{cases} U_l & \text{if} \quad x < 0 \\ U_r & \text{if} \quad x > 0 \end{cases} \tag{5}$$

where (U_l, U_r) represents the left and right element data values about a particular face, with local coordinate $x = 0$ at time $t = 0$, in the frame normal to that face. We denote the solution to this RP by $U^*(U_l, U_r; x/t)$. The solution is self similar in the x/t plane, being constant along rays through the origin. Through the rotational invariance of the Euler equations we may define the numerical flux in the frame normal to the face to be:

$$\mathbf{F}_k.\mathbf{n}_k = \mathbf{R}^{-1} H(\mathbf{R}U^*(U_l, U_r; 0)) \tag{6}$$

Here $\mathbf{R}$ is the rotation matrix constructed from the Euler angles associated with the face normal vector and H is the z direction Euler flux, and the RP solution is taken along the ray $t = 0$. If piecewise constant data is use for the left and right data states then this is simply the first order upwind Godunov flux. This scheme is extended to second order accuracy by the use of piecewise linear data reconstructions within each element of the MUSCL type, with the left and right data states now representing face-interpolated variable values. The scheme is constructed in three stages. First a slope limited central difference gradient plane is fitted through the four surrounding tetrahedral neighbour elements. This gradient plane is limited to be the maximum possible which does not produce undershoots or overshoots in the primitive field variables when interpolated to the inter-element face centroid positions. This extends to 3D the limiter described in [2]. Second these limited face interpolated data values are used to perform a non-conservative predictor type update - the "Hancock step" [12]- on the data values within each element:

$$U_i^{n+1/2} = U_i^n - \frac{\Delta t/2}{V_k} \sum_{k=0}^{3} A_k \mathbf{F}_k^+.\mathbf{n}_k \tag{7}$$

where the sum is again over the k faces of the element i. The $\mathbf{F}_k^+$ represents here the analytic flux $F\mathbf{i} + G\mathbf{j} + H\mathbf{k}$ evaluated on the element i data state interpolated to each interelement face centroid. The third stage in the construction of the numerical flux is to interpolate from the predicted data at the half timestep $U_i^{n+1/2}$ to each element face centroid, then use the left and right interpolated data states as initial data in the interelement RP. The numerical flux is then calculated from (6) as described above. The time step is decided by applying a CFL like condition based on an estimate of the maximum wave speed and element geometry. Implicit in this numerical method is the need to solve the RP for the Euler equations at each element interface at each time step. Rather than solve these inter-element RPs exactly which is computationally expensive, a computationally inexpensive approximate Riemann solver is employed. We use the HLLC approximate solver which is an improved version of the HLL solver of Harten, Lax and van Leer [5], and is obtained by incorporating the contact surface and shear waves into the wave pattern [11]. The HLLC solver has been extensively tested and shown to be both robust, accurate and computationally inexpensive [11].

4 MESH ADAPTATION ALGORITHM

The mesh refinement algorithm for TETRahedral ADaptivity (TETRAD) extends into the 3D prior work on 2D triangular meshes [3]. The approach we take is hierarchical in nature and and is based around *node*,*edges*,*face* and *element* objects which together

form the mesh data structure. The adaption algorithm assumes that an initial good quality tetrahedral mesh has been generated over the computational domain. and which will act as the invariant base mesh. This base mesh is then adapted in an h-refinement manner by node addition resulting in edge and element subdivision. For reasons of both tetrahedral quality control and algorithmic simplicity we allow only two types of element subdivision. The first, which we call *regular subdivision*, is the popular subdivision by eight across the longest interior diagonal of the parent tetrahedron [8], where a new node bisects each edge of the parent element. The second, which we call *green subdivision* [1], introduces an extra node into the parent tetrahedron, which is subsequently connected to all the parent vertices and any additional nodes which bisect the parent edges [7]. This provides a means of removing 'hanging nodes' without the introduction of additional edge refinement. Because these 'green tetrahedra' may be of poorer quality than their regular counterparts, when green tetrahedra flagged for refinement they are replaced by regularly refined tetrahedra. This requirement together with a recent result of Ong [10], means that the degradation of the mesh quality due to the refinement process is bounded. This approach has several advantages. First the algorithm is strongly local in nature which aids its parallellization. Second the green tetrahedra form interfaces between levels of refinement, making it straightforward to apply hierarchical adaptive time refinement and a multigrid implementations. The refinement and derefinement processes are driven from the action of refining and derefining element edges as suggested in [4]. Elements connecting to edges targeted for refinement or derefinement are adapted provided they pass various conditions which effectively decouple the regions of mesh refinement from those of derefinement. The various mesh objects edges, elements and so on are defined by their constituent nodes, with the key connectivity stored in the mesh data structure being that of which elements connect to a given mesh node in the form of a linked list. Nodes, edges and faces are also stored as lists, whereas elements are stored as trees. Only boundary faces are supported explicitly in the data structure. Scalability tests on the algorithm show the refinement process generates tetrahedra at the rate of 10500 per CPU second on a SGI R4400 processor, scaling as $O(N^{1.04})$ in mesh element number N. Full refinement/derefinement shock propagation tests show a scaling behaviour of $O(N^{1.14})$ in mesh size, which is encouraging but we believe can still be further improved . To combine the Euler flow solver with the adaptive algorithm currently we choose a simple flow variable approach which is sufficient for this application. Regions of the mesh of (low) high density gradient are flagged for (de)refinement, with the calculation of local flow gradients being performed across element faces. All the elements associated with a flagged face are flagged.

5 RESULTS AND CONCLUSION

The numerical simulations studied consist of shock wave diffraction around the 3D right angled corner formed between two cuboid mesh regions, in the 3D analogue of the 2D case studied in [6]. The initial mesh is generated by hexagonal cell subdivision into 5184 tetrahedral elements, with the first cuboid domain having dimensions $0.2 \times 0.2 \times 0.15$. Rankine-Hugoniot shock data initialises the computation, with the first cuboid domain being set to the post-shock data state and the discontinuity lying on the $x = 0.2$ plane. The ambient state has density $1.3 KgM^{-3}$ and pressure $100000 Pa$. We show here results of two computations, the first (Figures 1 and 2) being for a Mach 3.0 shock, and the second (Figure 3) for a Mach 1.7 shock. Figure 1 shows the surface of the computational mesh for the Mach 3 calculation, with 'O' marking the origin. The

shock has diffracted outwards through the square box section, with reflective boundary conditions in the $y = 0$ and $z = 0$ planes effectively dividing the computational problem by four. Figure 2 shows two cut planes through the solution at $z = 0.05$ (left picture) and $z = 0.2$ (the planes "aaa" and "bb" in Figure 1 respectively), giving 35 contours of density at an output time of $0.143mS$. A CFL number of 0.75 was used throughout. The final mesh contains 267323 elements with 3 levels of adaption being employed. The solution shows the recompression shock surface expected from the 2D calculations [6], with the $z = 0.2$ plane cutting along and across the shock surface, which forms a band around the $x = 0.2$ square section entrance. A region of low density and pressure separated flow exists 'behind' the corner. Diffraction effects in the z direction can be seen from the relative position of the shock on the two cut planes. Figure 3 shows the results of the Mach 1.7 density calculations along the same solution cut planes. Here the post shock flow is subsonic and causes the strong vortical activity in the region behind the box section entrance. Arrow plots of absolute velocity and examination of the vorticity vector confirms the presence of a ring vortex in this region of radius between $0.01M$ and $0.02M$. Preliminary measurements of the vortical circulation Γ and vortical Mach number $M_\Gamma = \Gamma/2\pi a_\infty$, where we have taken a_∞ to be the post-shock sound speed, gives M_Γ in the filament to be approximately 0.75, with estimated speed of the ring as $100MS^{-1}$ to $120MS^{-1}$. Moore's relation between ring velocity and vortical Mach number [9], based on a idealised ring vortex structure, predict a ring velocity of approximately $20MS^{-1}$ to $45MS^{-1}$ for this M_Γ. Given the preliminary nature of these measurements as well as the box section geometry, it is interesting that this agreement is so good. Further work on this is in progress. The computations were carried out on a SGI 8 processor Power Challenge machine with $256MB$ physical memory and took approximately 900 CPU minutes.

ACKNOWLEDGEMENT

This work was sponsored by the Pervasive Technology Department at Shell Research Ltd, Thornton Research Cenre, UK.

References

[1] R.E. BANK *PLTMG user's guide, edition 4.0*,Technical report, Department of Mathematics, University of California, San Diego, 1985.

[2] P. BATTEN AND D.M CAUSON, *Positively conservative high resolution convection schemes for unstructured elements* Submitted to Int. J. Num. Meth. Eng.

[3] M. BERZINS, J.WARE AND J.LAWSON, Advances in Comp. Meths. for PDE's. IMACS PDE VII.IMACS, 1992.

[4] R. BISWAS AND R. STRAWN, AIAA-93-0672, Reno 1993.

[5] A. HARTEN, P.D LAX AND B. VAN LEER, SIAM Rev. 25, 1983, 36-61

[6] R. HILLIER, Shock Waves 1, 1991, 89-98.

[7] Y. KALLINDERIS,V. PARTHASARATHY,AND J. WU, AIAA 92-0446, Reno 1992.

[8] R. LOHNER AND J.D. BAUM, J. Num. Meth. Fluids,14, 1992, 1407-1419.

[9] D.W MOORE, Proc. Royal Society A 397, 1987.

[10] M.E.G ONG, SIAM J. Sci. Comp. 15, 5, 1994.

[11] E.F TORO, M. SPRUCE AND W.SPEARES, Shock Waves 4, 1994, 25-34.

[12] B. VAN LEER, SIAM J. of Sci. and Stat. Comp. 5, 1984.

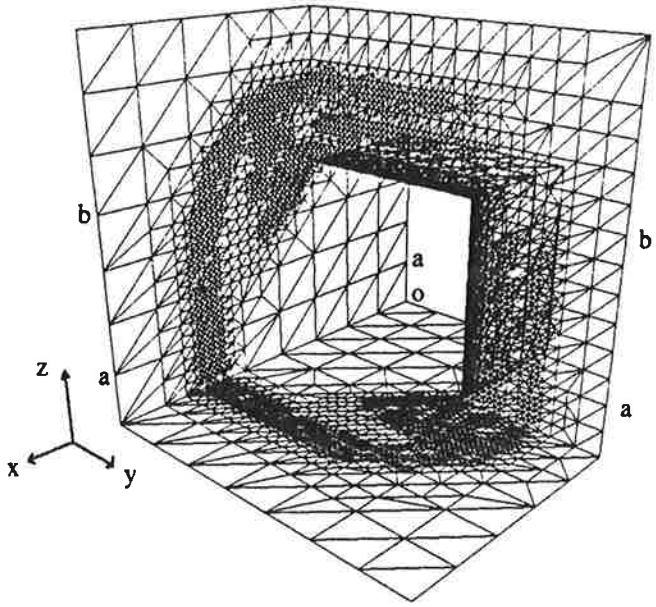

Figure 1: Mach 3 solution adapted mesh

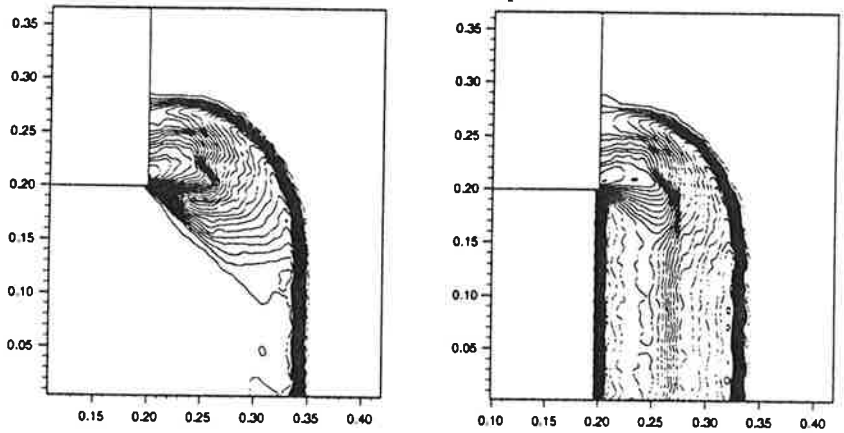

Figure 2: Mach 3.0 density (35 contours) $Z = 0.05$ and $Z = 0.2$ cut planes

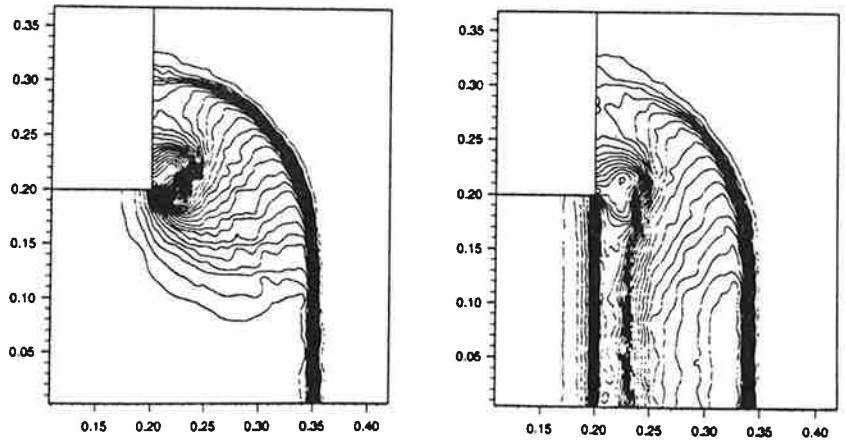

Figure 3: Mach 1.7 density (35 contours) $Z = 0.05$ and $Z = 0.2$ cut planes